Separable recruitment of DNA Polymerase α for leading- and lagging-strand replication initiation

Sarina Y. Porcella[1], Natasha C. Morse[1], Colin P. Tang[1,2], Priyanka Srivastava[1,3], Duncan J. Smith[1,4]

1. Department of Biology, New York University, New York, NY 10003, USA

2. Present address: Weill-Cornell Graduate School of Medical Sciences, New York, NY 10065, USA

3. Present address: School of Dentistry, UCSF Center for the Health Sciences, San Francisco, CA 94143

4. Corresponding author: duncan.smith@nyu.edu

Keywords: DNA replication, Lagging-strand synthesis, Replication origins, Checkpoint activation

ABSTRACT

During eukaryotic DNA replication, DNA polymerase alpha/primase (Pol α) initiates synthesis on both the leading and lagging strands. It is unknown whether leading- and lagging-strand priming are mechanistically identical, and whether Pol α associates processively or distributively with the replisome. Here, we titrate cellular levels of Pol α in *S. cerevisiae* and analyze Okazaki fragments to study both replication initiation and ongoing lagging-strand synthesis *in vivo*. We find that leading- and lagging-strand initiation are differentially sensitive to Pol α abundance, and to the presence of the replisome adaptor protein Ctf4. Our results suggest that distinct, distributive modes of Pol α recruitment exist for the leading and lagging strands. Additionally, we observe that activation of the checkpoint becomes essential for viability upon severe depletion of Pol α, and demonstrate that this checkpoint requirement is due to impaired leading-strand initiation as opposed to reduced lagging-strand priming.

32 **INTRODUCTION**

33

34 DNA polymerase alpha/primase (Pol α) is responsible for initiating synthesis on the leading
35 strand and for each Okazaki fragment on the lagging strand (Kunkel and Burgers, 2008). The
36 ultimate contribution of Pol α to replication is limited, and bulk synthesis on the leading- and
37 lagging-strands is carried out by DNA polymerase epsilon (Pol ε) and polymerase delta (Pol δ),
38 respectively (Clausen et al., 2015; Daigaku et al., 2015; Pursell et al., 2007; Reijns et al., 2015).
39 Despite the fact that different DNA polymerases carry out the majority of DNA synthesis on the
40 two daughter strands, Pol α appears to hand off synthesis predominantly to Pol δ during normal
41 initiation on both strands and during replication restart (Daigaku et al., 2015; Garbacz et al.,
42 2018; Yeeles et al., 2017; Miyabe et al., 2015). The use of the same initiating polymerase and
43 downstream partner implies a possible similarity between leading- and lagging-strand initiation.
44 However, recent analysis of repriming during damage bypass by reconstituted replisomes
45 provides evidence that leading- and lagging-strand repriming are mechanistically distinct
46 processes (Taylor and Yeeles, 2018).

47

48 Eukaryotic Okazaki fragments are considerably shorter than their prokaryotic counterparts
49 (Balakrishnan and Bambara, 2013; Ogawa and Okazaki, 1980). Okazaki fragment length is
50 quantized by the nucleosome repeat via interactions between nascent nucleosomes and Pol δ
51 in *S. cerevisiae* (Smith and Whitehouse, 2012) and *C. elegans* (Pourkarimi et al., 2016).
52 Okazaki fragment termini can also be positioned by nucleosomes in a reconstituted *S.*
53 *cerevisiae* replication reaction (Devbhandari et al., 2017). Both the distribution of Okazaki
54 fragment termini with respect to nucleosomes and the overall length profile of lagging-strand
55 products in *S. cerevisiae* and *C. elegans* are remarkably similar. Despite this apparent size

56 conservation, Okazaki fragment length can be altered on a non-chromatinized template *in vitro*
57 by varying the concentration of Pol α (Kurat et al., 2017), analogous to the impact of primase
58 titration on lagging-strand synthesis in a reconstituted *E. coli* replication system (Wu et al.,
59 1992). Eukaryotic Okazaki fragment length can also be increased *in vivo* by impairing
60 nucleosome assembly (Smith and Whitehouse, 2012; Yadav and Whitehouse, 2016).
61
62 The maximum length of an Okazaki fragment is determined by the amount of single-stranded
63 DNA unwound at the replication fork before lagging-strand priming and extension. Thus, longer
64 fragments would result in the exposure of long stretches of damage-prone single-stranded DNA.
65 Shorter Okazaki fragments would expose shorter stretches of ssDNA, but at the likely cost of
66 increasing the contribution of the error-prone Pol α to synthesis of the lagging daughter strand
67 (Kunkel, 2011; Reijns et al., 2015). However, it is currently unclear to what extent changing
68 Okazaki fragment length directly impacts cellular fitness. Reduced DNA polymerase activity
69 upon aphidicolin treatment induces chromosome breakage and genomic rearrangements at
70 fragile sites in mammals (Glover et al., 1984). Analogously, reducing the intracellular
71 concentration of Pol α in *S. cerevisiae* increases S-phase duration, sensitivity to DNA damaging
72 agents, and chromosomal rearrangements at defined sites (Lemoine et al., 2005; Song et al.,
73 2014). The detrimental effects of Pol α depletion on genome integrity could arise due to
74 defective leading- or lagging-strand initiation, both of which are dependent on Pol α.
75
76 Ctf4 was originally identified as a chromosome transmission fidelity mutant (Kouprina et al.,
77 1992). Subsequent studies have identified multiple roles for Ctf4 in DNA metabolism. Ctf4 is not
78 only required for the establishment of sister chromatin cohesion (Borges et al., 2013; Hanna et
79 al., 2001), but also links Pol α to the replication fork via interaction with the replicative helicase

80 (Gambus et al., 2009; Tanaka et al., 2009), and is additionally required for error-free lesion
81 bypass (Fumasoni et al., 2015) and rDNA maintenance (Villa et al., 2016). At least some of
82 these roles for Ctf4 are independent of Pol α binding. The metazoan Ctf4 ortholog AND-1 also
83 stimulates Pol α binding to chromatin, and is required for efficient DNA replication (Zhu et al.,
84 2007). Interestingly, despite the conserved contribution of Ctf4 to Pol α recruitment, *ctf4Δ S.*
85 *cerevisiae* strains have been demonstrated to synthesize identically sized Okazaki fragments to
86 wild-type cells (Borges et al., 2013). *In vitro*, the Ctf4 protein has a minimal effect on the priming
87 of either DNA strand in reconstituted replication reactions (Kurat et al., 2017). Thus, the
88 contribution of Ctf4 to leading- and lagging-strand priming has not been fully elucidated *in vivo*.
89
90 Here, we analyze Okazaki fragments to directly test the effects of Pol α depletion on leading-
91 and lagging-strand initiation in *S. cerevisiae*. We find that Pol α is recruited distributively to the
92 replication fork for priming on both strands, but that only lagging-strand priming is dependent on
93 Ctf4. Impaired lagging-strand priming is well tolerated, but reduced leading-strand initiation
94 leads to a strict dependence on checkpoint activation for continued viability.
95
96 **RESULTS**
97
98 **Cells with reduced levels of Pol α synthesize longer Okazaki fragments *in vivo.***
99
100 To investigate the effect of Pol1 depletion on leading- and lagging-strand priming during
101 replication, we modified the approach of Petes and co-workers (Lemoine et al., 2005; Song et
102 al., 2014), limiting expression of *POL1* by replacing its promoter with *pGAL1*. Expression of Pol1
103 from galactose-inducible promoters generates a stable polypeptide that can persist for several

104 cell cycles (Muzi Falconi et al., 1993). Therefore, to facilitate turnover of pre-existing Pol1 and
105 focus on the acute effects depletion, we additionally fused an N-terminal degron to the *POL1*
106 coding sequence. Western-blot analysis indicated that the concentration of this GAL1-
107 expressed, degron-tagged Pol1 (GDPol1) could be specifically and rapidly modulated within 4h
108 (Fig. 1A). All cultures were grown in media supplemented with 3% raffinose to avoid indirect
109 effects due to carbon limitation. Pol1 levels oscillate through the cell cycle when the protein is
110 endogenously expressed, but not when expression is driven by galactose (Muzi Falconi et al.,
111 1993). Because Pol1 concentration is not constant even within S-phase (Muzi Falconi et al.,
112 1993), and 2/3 of cells in an asynchronous population are in G1, G2 or M phase, precise
113 comparisons of Pol1 concentration between galactose-inducible and endogenously expressed
114 conditions are unreliable. We estimate that the expression level at 0.05% galactose is slightly
115 lower than endogenous during the relevant phase of the cell cycle.
116
117 To analyze Okazaki fragment biogenesis, we crossed the *GDPOL1* allele into a strain
118 background in which DNA ligase I (Cdc9) can be depleted from the nucleus by rapamycin
119 treatment using the anchor away method (Haruki et al., 2008). Nuclear depletion of Cdc9
120 enriches nucleosome-sized Okazaki fragments (Fig. S1A), similarly to transcriptional repression
121 of Cdc9 (Smith and Whitehouse, 2012; Yadav and Whitehouse, 2016). Robust detection of
122 Okazaki fragments was possible after 1h rapamycin treatment: therefore, all Okazaki fragment
123 labeling and sequencing experiments were conducted after a 4h sugar switch to reduce Pol α
124 levels, followed by 1h ligase depletion by rapamycin (Fig. 1B).
125
126 By end labeling unligated Okazaki fragments, we observed that cells with wild-type *POL1* did
127 not show an increase in Okazaki fragment length under low-galactose growth conditions (Fig.
128 1C). By contrast, in the *GDPOL1* strain Okazaki fragment length was normal at Pol1

129 concentrations down to a critical concentration corresponding to growth in 0.014% galactose
130 (Fig. 1D). At 0.014% galactose the Okazaki fragment length profile was shifted slightly upwards
131 such that fragments were clearly still phased by nucleosomes, while lower galactose
132 concentrations (0.005%) showed a significant loss of signal (Fig. 1D cf. lanes 5&6). To confirm
133 that this loss of signal reflected a further length increase (and therefore a reduction in the
134 number of ends being labeled), we analyzed Okazaki fragments by Southern blot using a whole-
135 genome probe: as anticipated for severely perturbed lagging-strand priming, Okazaki fragments
136 at 0.005% galactose were significantly larger than at 0.014% (Fig. 1E). We conclude that
137 limiting levels of Pol α lead to reduced priming frequency on the lagging strand, resulting in
138 longer Okazaki fragments, and that *S. cerevisiae* cells can sustain growth when Okazaki
139 fragment length is substantially increased. Further, these data are consistent with the repeated,
140 distributive recruitment of Pol α to the replisome for lagging-strand priming during replication,
141 since the priming kinetics of a Pol α complex stably associated with the replisome would be
142 unaffected by cellular Pol α concentrations (see discussion).
143
144 To analyze the location of Okazaki fragment termini, we purified and sequenced Okazaki
145 fragments (Smith and Whitehouse, 2012) from wild-type and *GDPOL1* strains shifted to low
146 galactose concentrations for 4h before 1h ligase depletion. Galactose concentration does not
147 significantly affect the distribution of Okazaki fragment termini in wild-type cells (Fig. 1F).
148 However, we observed that fragment termini in *GDPOL1* cells were no longer enriched at
149 nucleosome dyads during growth in 0.005% galactose. Instead, the distribution was flattened
150 and termini were preferentially found upstream of the nucleosome dyad (Fig. 1G). An
151 intermediate effect is observed at 0.014% galactose. Pol1 interacts with the FACT component
152 Spt16 (Foltman et al., 2013) Therefore, the change in the distribution of Okazaki fragment ends

153 upon severe Pol α depletion could plausibly arise due to defects in chromatin assembly as
154 observed in histone chaperone mutants (Smith and Whitehouse, 2012; Yadav and Whitehouse,
155 2016). An alternative, though not mutually exclusive, possibility is that Okazaki fragment
156 processing is impaired when priming frequency is reduced.
157
158 **Reduced levels of Pol α lead to a global decrease in replication origin firing efficiency**
159
160 Replication origin firing efficiency can be quantitatively inferred from the distribution of Watson-
161 and Crick-strand Okazaki fragments after deep sequencing (McGuffee et al., 2013; Petryk et al.,
162 2016; Pourkarimi et al., 2016). Okazaki fragment distributions on the right arm of chromosome
163 10 are shown in Fig. 2A, and genome-wide origin efficiencies are quantified in Fig. 2B.
164 Correlations between replicate datasets were robust, although one replicate at 0.032%
165 galactose produced systematically low origin efficiencies (Fig. S2A). Data in Fig. 2 represent the
166 mean origin efficiency across two replicate experiments. While origin efficiency was unaffected
167 by galactose concentration in wild-type cells, average firing efficiency was linearly reduced in
168 the *GDPOL1* strain at progressively lower galactose concentrations (Fig. 2B).
169
170 Interestingly, we observe that the efficiency of leading-strand priming is already substantially
171 reduced at Pol1 concentrations below the endogenous expression level that still support normal
172 lagging-strand priming. Unlike lagging-strand priming, which is robust to reduction in Pol1 levels
173 down to a critical concentration, leading-strand priming efficiency is sensitive to even small
174 changes in Pol α concentration. At 0.041%, 0.032% and 0.023% galactose, Pol1 expression is
175 sufficient for unperturbed lagging-strand synthesis but median origin efficiency is significantly
176 reduced in the *GDPOL1* strain (Fig. 2B). Further reduction is observed at lower galactose (and

177 therefore Pol1) concentrations. This dramatic decrease in origin efficiency likely contributes to
178 the slow growth (Fig. S1B) and cell-cycle delay (Lemoine et al., 2005) observed under limiting
179 Pol1 conditions. Even at low Pol1 concentrations, we observe no change in fork arrest at tDNAs
180 (Fig. S3) – the major sites of replisome stalling in the *S. cerevisiae* genome (Ivessa et al., 2003;
181 Osmundson et al., 2017). Thus, the altered replication profile upon Pol1 depletion most likely
182 stems exclusively from changes in origin efficiency with no additional effects due to replication-
183 fork stalling or arrest.
184
185 If one or more Pol α complexes is stably recruited to and maintained in the replisome upon
186 leading-strand priming, reducing Pol α to sub-stoichiometric levels would privilege early and/or
187 efficient replication origins while disproportionately reducing the efficiency of late and/or
188 inefficient origins. By contrast, distributive recruitment would lead to reduced efficiency of all
189 origins under limiting Pol α conditions. We analyzed origin efficiency in the *GDPOL1* strain as a
190 function of normal firing efficiency. As the concentration of Pol α was decreased, firing of all
191 origins became less efficient regardless of their normal efficiency (Fig. 2C and S2B). Further
192 analysis indicated that the activity of each origin is reduced in proportion to its original firing
193 efficiency (Fig. 2D). These data, along with the reduced lagging-strand priming frequency under
194 limiting Pol α conditions shown in Fig. 1, support a model where Pol α associates distributively
195 with the replisome for both leading- and lagging-strand priming.
196
197 **Ctf4 stimulates Pol α recruitment for lagging-strand but not leading-strand priming**
198
199 Ctf4 has previously been shown to stimulate the recruitment of Pol α and several additional
200 proteins to the replisome (Gambus et al., 2009; Samora et al., 2016; Tanaka et al., 2009; Villa et

201 al., 2016). Indeed, it has been proposed that a Ctf4 homotrimer could simultaneously recruit two
202 Pol α complexes while the third Ctf4 subunit is tethered to the replisome via interaction with the
203 Sld5 component of the Cdc45/MCM2-7/GINS (CMG) complex (Simon et al., 2014). *CTF4* is
204 nonessential in *S. cerevisiae*; the absence of Ctf4 does not affect lagging-strand synthesis in a
205 reconstituted *S. cerevisiae* replication system (Kurat et al., 2017), and Okazaki fragment length
206 is unchanged in otherwise wild-type *ctf4Δ* cells (Borges et al., 2013). To investigate the effect of
207 Ctf4 on leading- and lagging-strand synthesis under limiting Pol α conditions, we analyzed
208 Okazaki fragments from strains deleted for *CTF4* using Southern blots and sequencing.
209
210 In the absence of Ctf4, Okazaki fragments increase in length at ~0.06% galactose (Fig. 3A,)–
211 significantly higher than the 0.014% observed for a *CTF4* wild-type strain (cf. Fig. 1D&E).
212 Continued growth while synthesizing long Okazaki fragments was observed down to 0.005%
213 galactose (Fig. B), with a significant reduction in viability observed only at the lowest
214 concentration tested (0.005%; Fig. S4A). It has previously been demonstrated that overall
215 cellular levels of Pol1 are unaffected by the absence of, or a failure to bind, Ctf4 (Villa et al.,
216 2016). Our data therefore suggest that Ctf4 helps to maintain robust lagging-strand priming
217 when Pol α activity is reduced, although cellular levels of Pol α are sufficient for normal lagging-
218 strand priming even in its absence (Fig. 3A and (Borges et al., 2013)).
219
220 We analyzed replication origin firing efficiency in the absence of Ctf4 by sequencing Okazaki
221 fragments from a *ctf4Δ* strain grown at various galactose concentrations (Fig. 3C). Data shown
222 are the average of two replicates (with the exception of 0.032% galactose, for which a single
223 replicate was sequenced). Correlations between replicates were extremely robust (Fig. S4C). In
224 contrast to the *CTF4* strain (Fig. 2B), *ctf4Δ* cells maintained normal levels of origin firing down to

225 0.032% galactose, after which a linear decrease in firing efficiency was apparent (Fig. 3C).
226 Surprisingly, firing efficiency for all origins was significantly higher in the *ctf4Δ* strain relative to
227 *CTF4* across all galactose concentrations tested (Fig. 3D).
228
229 Each rDNA repeat in *S. cerevisiae* contains a replication origin. rDNA size has been reported to
230 change due to deletion of *CTF4* (Sasaki and Kobayashi, 2017) or lithium acetate transformation
231 (Kwan et al., 2016). Expansion of the rDNA repeat increases the total number of origins in the
232 genome, and could thereby depress origin firing elsewhere (Shyian et al., 2016; Yoshida et al.,
233 2014). We investigated whether the increased origin efficiency in *ctf4Δ* cells could be an artifact
234 due to a reduction in the size of the rDNA array. The proportion of Okazaki fragments mapping
235 to the rDNA in *ctf4Δ* libraries was around 70% higher than in *CTF4* libraries (Fig. S4B),
236 consistent with substantial array expansion in the absence of Ctf4 (Sasaki and Kobayashi,
237 2017). Therefore, the global increase in origin efficiency in the absence of Ctf4 is extremely
238 unlikely to be driven by rDNA copy number changes.
239
240 We conclude that Ctf4-mediated recruitment of Pol α to the replisome does not stimulate
241 leading-strand priming in *S. cerevisiae*, but plays an important role in maintaining the
242 robustness of lagging-strand priming to fluctuations in the availability of Pol α. In the absence of
243 Ctf4, Pol α is no longer sequestered to active replication forks (Villa et al., 2016). Consequently,
244 more Pol α is available to initiate leading-strand synthesis via Ctf4-independent recruitment, and
245 normal origin firing can be maintained at low overall concentrations of Pol α.
246
247 **Checkpoint activation is required for viability when origin firing is reduced, but not when**
248 **lagging-strand priming is perturbed**

249

250 In response to DNA damage or replication stress, a checkpoint signaling cascade is initiated
251 and culminates in the phosphorylation of the effector kinase Rad53 (Ciccia and Elledge, 2010).
252 We analyzed Rad53 phosphorylation in the *GDPOL1* strain after a switch to low galactose.
253 Substantial phosphorylation of Rad53 was observed only at concentrations below 0.023%
254 galactose (Fig. 4A) – a concentration at which both leading- and lagging-strand initiation are
255 perturbed (Figs. 1&2). To further investigate the interplay between Pol α depletion, increased
256 Okazaki fragment length, decreased origin firing, and checkpoint activation, we combined the
257 *GDPOL1* allele with deletion of *MEC1* (with additional deletion of *SML1* to maintain viability of
258 *mec1Δ* cells). *GDPOL1* and *mec1Δ;sml1Δ* mutant strains grew well at galactose concentrations
259 from 0.05% to 0.005%, but growth of the *GDPOL1; mec1Δ; sml1Δ* mutant was impaired at
260 0.05% galactose and virtually absent at 0.014% and 0.005% galactose (Fig. 4B). Thus,
261 checkpoint-deficient cells apparently cannot survive with limiting Pol α. Consistent with a rapid
262 loss of viability upon Pol1 depletion in checkpoint-deficient cells, we were unable to robustly
263 detect long Okazaki fragments in *GDPOL1; mec1Δ; sml1Δ* cells shifted to low concentrations of
264 galactose (Fig. 4C). Okazaki fragment length was normal in this strain at galactose
265 concentrations above 0.023%.

266

267 To test the contributions of the DNA damage checkpoint (DDC), mediated by Rad9, and the
268 DNA replication checkpoint (DRC), mediated by Mrc1, to survival under limiting Pol α
269 conditions, we analyzed the growth of *GDPOL1* strains in combination with *rad9Δ*, *mrc1Δ*, or the
270 non-phosphorylatable *mrc1*^{AQ} allele (Osborn and Elledge, 2003) (Fig. 4B). *GDPOL1* cells
271 showed robust growth at low Pol1 concentrations in both *rad9Δ* and *mrc1Δ* strain backgrounds.
272 *GDPOL1;mrc1*^{AQ} cells grow as well as *GDPOL1* cells at all concentrations tested. Therefore, the

273 slight growth defect at 0.005% galactose observed in *GDPOL1;mrc1Δ* cells is most likely due to
274 decreased replication fork speed (Szyjka et al., 2005; Yeeles et al., 2017) in combination with
275 decreased origin firing (Fig. 2B) as opposed to impaired DRC activity. In summary, checkpoint
276 activation is required for viability under conditions of severe Pol α depletion: this activation can
277 proceed via either the DDC or the DRC.
278
279 To determine whether the requirement for checkpoint activation was due to deregulated lagging-
280 strand priming or impaired leading-strand initiation, we compared the growth of
281 *GDPOL1;mec1Δ;sml1Δ* strains with and without *CTF4* at 0.5% and 0.05% galactose. Deletion of
282 *CTF4* affects lagging-strand priming at relatively high Pol α concentrations, before leading-
283 strand priming is impaired. Thus, *ctf4Δ* is effectively a separation of function mutant: at 0.05%
284 galactose, lagging-strand priming is reduced by the absence of Ctf4 while leading-strand
285 priming is not (Fig. 3). *GDPOL1;mec1Δ;sml1;Δctf4Δ* cells grow slowly relative to *MEC1* or *CTF4*
286 cells: however, growth was essentially unaffected by reducing the galactose concentration from
287 0.5% to 0.05% (Fig. 4D). Therefore, perturbed lagging-strand synthesis does not directly cause
288 growth defects the absence of a functional checkpoint. We conclude that cells with limiting Pol α
289 become reliant on the checkpoint predominantly due to decreased replication origin firing as
290 opposed to increased Okazaki fragment length.
291
292 **DISCUSSION**
293
294 **Cellular impact of perturbed leading- and lagging-strand initiation.**
295

296 We find that checkpoint activation is required for robust DNA synthesis, and therefore for
297 viability, when origin firing is significantly reduced (Fig. 4). This observation is consistent with
298 genetic interactions in *S. cerevisiae* – for example similar negative genetic interactions of *rad9Δ*
299 with alleles of the catalytic subunits of each of the three replicative polymerases (Dubarry et al.,
300 2015). It will be interesting to determine the contributions of leading- and lagging-strand
301 perturbations to the many reported phenotypes resulting from *pol1* mutation or Pol1 depletion –
302 for example increased trinucleotide repeat expansion rate and size (Shah et al., 2012), and
303 increased chromosome fragility (Lemoine et al., 2005; Song et al., 2014). Furthermore,
304 mutations that reduce the levels of functional Pol ε in mammalian cells increase replication
305 stress linked to reduced origin firing (Bellelli et al., 2018), highlighting the relevance of these
306 studies beyond budding yeast.
307
308 **Pol α priming on the leading- and lagging strands**
309
310 Our data indicate that lagging-strand priming in *S. cerevisiae* is extremely robust with respect to
311 fluctuations in Pol α availability. Pol α concentration does not normally limit primer synthesis
312 and/or utilization, and significant disruption of Okazaki fragment synthesis is only observed at
313 very low Pol α concentrations (Fig. 1). Because cells with limiting Pol α synthesize longer
314 Okazaki fragments, as opposed to fewer Okazaki fragments of normal size, Pol α must act
315 distributively *in vivo* as opposed to being stably tethered at the replication fork. We additionally
316 note that the increase in Okazaki fragment length upon Pol α depletion is consistent with a
317 priming mechanism in which there is no strict coupling between DNA unwinding and primer
318 synthesis *in vivo*.
319

320 Although the Ctf4 protein has little to no effect on lagging-strand synthesis in chromatinized
321 reconstituted systems (Kurat et al., 2017), we observe that Ctf4 stimulates lagging-strand
322 priming *in vivo*. In the absence of Ctf4, Okazaki fragment length can still be modulated by Pol α
323 concentration (Fig. 3). Thus, in light of the distributive action of Pol α, Ctf4 presumably acts
324 simply by increasing the local concentration of Pol α at the replication fork. It is unclear what
325 underlies the differential Ctf4-sensitivity of reconstituted and *in vivo* lagging-strand synthesis.
326
327 Neither leading- nor lagging-strand priming is limited by Pol α at normal cellular concentrations
328 of the complex. However, leading-strand initiation is substantially more sensitive than lagging-
329 strand priming to fluctuations in Pol α (Figs 1&2). Our data indicate not only that origin firing
330 efficiency decreases at Pol α concentrations that do not significantly affect priming frequency,
331 but also that Ctf4-mediated recruitment of Pol α to elongating replication forks can directly
332 decrease origin activity (Fig. 3 and model, Fig. 5). This competition between replication initiation
333 and elongation might represent a simple homeostatic mechanism that allows cells to decrease
334 the number of newly initiating replication forks in order to maintain robust synthesis at ongoing
335 forks.
336
337 We show that, unlike lagging-strand priming, initiation on the leading strand is independent of
338 Ctf4 *in vivo* (Figs. 2&3). This finding extends previous observations that leading-strand
339 repriming and lagging-strand priming respond differently to changes in RPA concentration
340 (Taylor and Yeeles, 2018), and identifies an additional mechanistic difference between the two
341 priming tasks performed by Pol α. It has been suggested that leading-strand initiation could
342 occur through Pol ε-mediated extension of the first Okazaki fragment synthesized on the lagging
343 strand (Taylor and Yeeles, 2018): the significant differences observed between leading-and

344 lagging-strand priming argue against this possibility, unless synthesis of the first Okazaki
345 fragment is itself different from ongoing lagging-strand synthesis. We note that, because we are
346 exclusively analyzing lagging-strand products, it is formally possible that uncoupled lagging-
347 strand synthesis is occurring in the absence of leading-strand synthesis after origin firing. We
348 believe that this is an unlikely scenario, as we do not observe a significant reduction in growth
349 rate or viability even when origin firing is reduced (Fig. S1B).
350
351 All replication origins are affected by Pol α depletion, in proportion to their normal firing
352 efficiency (Fig. 2D). A significant reduction in origin firing efficiency is observed at Pol1
353 concentrations that do not detectably activate the checkpoint (Figs. 2B & 4A); in addition, origin
354 firing efficiency is higher in *ctf4Δ* than *CTF4* cells at limiting Pol α. Therefore, it is unlikely that
355 the reduction in origin firing is a direct result of checkpoint activation. Our data suggest that the
356 origin firing program is determined by the relative accessibility of licensed origins to limiting
357 soluble firing factors, even when overall origin firing is reduced. Spatial clustering of replication
358 origins, mediated by Fkh transcription factors in *S. cerevisiae*, likely plays a significant role in
359 this accessibility (Knott et al., 2012). We note that coordinately down-regulating the efficiency of
360 all origins represents a robust strategy to maintain the evolutionarily selected co-orientation of
361 deleterious transcription events with replication (Hamperl and Cimprich, 2016; Osmundson et
362 al., 2017; Tran et al., 2017).
363
364 **Chromatin and lagging-strand synthesis**
365
366 Pol α acts distributively on naked DNA in reconstituted replication reactions (Yeeles et al.,
367 2017). Chromatin reduces Okazaki fragment size *in vitro,* and has therefore been proposed to

368 make Pol α more processive (Kurat et al., 2017). Our data suggest that Pol α acts distributively
369 on chromatin *in vivo*, but is present at saturating concentrations that would minimize the
370 difference between distributive or processive activity. Our data do, however, support an intimate
371 interaction between chromatin and lagging-strand priming. Extreme depletion of Pol α leads to
372 Okazaki fragment distributions consistent with impaired chromatin assembly (Fig. 1G). It is
373 possible that the increased length of Okazaki fragments reported in histone chaperone mutants
374 (Smith and Whitehouse, 2012; Yadav and Whitehouse, 2016) represents an underlying defect in
375 priming.
376

377 **MATERIALS AND METHODS**

378 **Yeast strains**

379 All yeast strains were W303 *RAD5+*, and contained additional mutations required for anchor-
380 away depletion of Cdc9. The genotype of the wild-type strain is *matα, tor1-1::HIS3,*
381 *fpr1::NatMX4, RPL13A-2xFKBP12::TRP1, CDC9-FRB::HygMX*. Additional gene deletions, and
382 replacement of the *POL1* promoter, were carried out by PCR-mediated replacement in a wild-
383 type strain, and introduced into the desired background by cross.
384

385 **Cell growth and spot tests**

386 All strains were grown at 30°C, starting in YEP with 0.5% galactose plus 3% raffinose, unless
387 otherwise noted. To deplete Pol1, cultures were sugar switched by growing overnight to log
388 phase then washing the cels with sterile deionized water then sterile YEP before being
389 inoculated into fresh YEP media with various galactose concentrations supplemented with 3%
390 raffinose.
391

392 For short-term experiments, strains were grown for four hours after the sugar switch before
393 adding rapamycin for one hour of ligase repression. Cells were collected four hours after the
394 sugar switch, without depletion of DNA ligase, for western blot analysis.
395 For spot tests, yeast cells were washed then counted. Similar numbers of cells were plated onto
396 various galactose concentrations at a 1:5 dilution series and grown overnight for two days at
397 30°C.
398
399 **Western blotting**
400 Samples were collected by centrifugation and washed with deionized water before lysate
401 preparation. Lysates were prepared by five-minute resuspension in 600uL 2M lithium acetate on
402 ice, pelleted, resuspended in 600uL 400mM sodium hydroxide at room temperature for five
403 minutes, pelleted, and resuspended in Laemmli buffer with 5% beta-mercaptoethanol prior to
404 boiling, then briefly pelleted immediately prior to loading the lysate onto a SDS-PAGE gel.
405 Samples were transferred to PVDF, blocked with 5% milk and probed with C-Myc antibody
406 (Genscript A00173-100), Rad53 antibody (Abcam ab104232), histone H4 antibody (Abcam
407 ab10158), or actin antibody (Thermofisher Scientific MA1-744).
408
409 **Okazaki fragment analysis by gel electrophoresis**
410 Okazaki fragments were purified and end-labeled as previously described (Smith and
411 Whitehouse, 2012). For southern blot analysis, unlabeled genomic DNA was normalized to total
412 genomic DNA, and run on 1.3% denaturing agarose gels. After electrophoresis, the gel was
413 blotted onto a nitrocellulose membrane (Fisher 45-000-932) overnight. Next the membrane was
414 crosslinked and washed, then hybridized overnight with a probe synthesized with random
415 hexamers labeling kit (Fisher 18187-013) and sheared genomic DNA. After two low stringency
416 washes, membranes were dried then exposed to phosphor screens

417

418 **Okazaki fragment sequencing and origin efficiency analysis**

419 Okazaki fragments were deep-sequenced as previously described (Smith and Whitehouse,
420 2012). Paired-end sequencing (2 × 75 bp) was carried out on an Illumina Next-seq 500 platform.
421 Origin efficiency metric analysis of predefined origins was done as previously described
422 (McGuffee et al., 2013) with the origin list from the same source.

423

424 **DATA AVAILABILITY**

425 Sequencing data have been submitted to the GEO under accession number GSE115897.

426

427 **ACKNOWLEDGEMENTS**

428 We thank the NYU Gencore for assistance with TapeStation and sequencing, and members of
429 the Smith lab for helpful discussions. This work was supported by grants from the NIH (R01
430 GM114340) and the Searle Scholars Program to D.J.S.

431

432 **AUTHOR CONTRIBUTIONS**

433 S.Y.P., N.C.M., C.P.T., and P.S. performed research, S.Y.P. and D.J.S. analyzed and
434 interpreted data. S.Y.P prepared figures. D.J.S. wrote the manuscript with assistance from
435 S.Y.P. D.J.S. supervised the study.

436

437 **COMPETING INTERESTS**

438 No competing interests exist.

439 **REFERENCES**

440 Balakrishnan, L., and Bambara, R. A. (2013). Okazaki fragment metabolism. Cold Spring Harb
441 Perspect Biol *5*, ; doi: 10.1101/cshperspect.a010173.

442 Bellelli, R., Borel, V., Logan, C., Svendsen, J., Cox, D. E., Nye, E., Metcalfe, K., O'Connell, S.
443 M., Stamp, G., Flynn, H. R., Snijders, A. P., Lassailly, F., Jackson, A., and Boulton, S. J. (2018).
444 Polε Instability Drives Replication Stress, Abnormal Development, and Tumorigenesis. Mol Cell
445 *https://doi.org/10.1016/j.molcel.2018.04.008,*

446 Borges, V., Smith, D. J., Whitehouse, I., and Uhlmann, F. (2013). An Eco1-independent sister
447 chromatid cohesion establishment pathway in S. cerevisiae. Chromosoma *122*, 121-134.

448 Ciccia, A., and Elledge, S. J. (2010). The DNA damage response: making it safe to play with
449 knives. Mol Cell *40*, 179-204.

450 Clausen, A. R., Lujan, S. A., Burkholder, A. B., Orebaugh, C. D., Williams, J. S., Clausen, M. F.,
451 Malc, E. P., Mieczkowski, P. A., Fargo, D. C., Smith, D. J., and Kunkel, T. A. (2015). Tracking
452 replication enzymology in vivo by genome-wide mapping of ribonucleotide incorporation. Nat
453 Struct Mol Biol *22*, 185-191.

454 Daigaku, Y., Keszthelyi, A., Muller, C. A., Miyabe, I., Brooks, T., Retkute, R., Hubank, M.,
455 Nieduszynski, C. A., and Carr, A. M. (2015). A global profile of replicative polymerase usage.
456 Nat Struct Mol Biol *22*, 192-198.

457 Devbhandari, S., Jiang, J., Kumar, C., Whitehouse, I., and Remus, D. (2017). Chromatin
458 Constrains the Initiation and Elongation of DNA Replication. Mol Cell *65*, 131-141.

459 Dubarry, M., Lawless, C., Banks, A. P., Cockell, S., and Lydall, D. (2015). Genetic Networks
460 Required to Coordinate Chromosome Replication by DNA Polymerases α, δ, and ε in
461 Saccharomyces cerevisiae. G3 (Bethesda) *5*, 2187-2197.

462 Foltman, M., Evrin, C., De Piccoli, G., Jones, R. C., Edmondson, R. D., Katou, Y., Nakato, R.,
463 Shirahige, K., and Labib, K. (2013). Eukaryotic replisome components cooperate to process
464 histones during chromosome replication. Cell Rep *3*, 892-904.

465 Fumasoni, M., Zwicky, K., Vanoli, F., Lopes, M., and Branzei, D. (2015). Error-Free DNA
466 Damage Tolerance and Sister Chromatid Proximity during DNA Replication Rely on the
467 Polalpha/Primase/Ctf4 Complex. Mol Cell *57*, 812-823.

468 Gambus, A., van Deursen, F., Polychronopoulos, D., Foltman, M., Jones, R. C., Edmondson, R.
469 D., Calzada, A., and Labib, K. (2009). A key role for Ctf4 in coupling the MCM2-7 helicase to
470 DNA polymerase alpha within the eukaryotic replisome. EMBO J *28*, 2992-3004.

471 Garbacz, M. A., Lujan, S. A., Burkholder, A. B., Cox, P. B., Wu, Q., Zhou, Z. X., Haber, J. E.,
472 and Kunkel, T. A. (2018). Evidence that DNA polymerase δ contributes to initiating leading
473 strand DNA replication in Saccharomyces cerevisiae. Nat Commun *9*, 858.

474 Glover, T. W., Berger, C., Coyle, J., and Echo, B. (1984). DNA polymerase alpha inhibition by
475 aphidicolin induces gaps and breaks at common fragile sites in human chromosomes. Hum
476 Genet *67*, 136-142.

477 Hamperl, S., and Cimprich, K. A. (2016). Conflict Resolution in the Genome: How Transcription
478 and Replication Make It Work. Cell *167*, 1455-1467.

479 Hanna, J. S., Kroll, E. S., Lundblad, V., and Spencer, F. A. (2001). Saccharomyces cerevisiae
480 CTF18 and CTF4 are required for sister chromatid cohesion. Mol Cell Biol *21*, 3144-3158.

481 Haruki, H., Nishikawa, J., and Laemmli, U. K. (2008). The anchor-away technique: rapid,
482 conditional establishment of yeast mutant phenotypes. Mol Cell *31*, 925-932.

483 Ivessa, A. S., Lenzmeier, B. A., Bessler, J. B., Goudsouzian, L. K., Schnakenberg, S. L., and
484 Zakian, V. A. (2003). The Saccharomyces cerevisiae helicase Rrm3p facilitates replication past
485 nonhistone protein-DNA complexes. Mol Cell *12*, 1525-1536.

486 Jiang, C., and Pugh, B. F. (2009). A compiled and systematic reference map of nucleosome
487 positions across the Saccharomyces cerevisiae genome. Genome Biol *10*, R109.

488 Knott, S. R., Peace, J. M., Ostrow, A. Z., Gan, Y., Rex, A. E., Viggiani, C. J., Tavare, S., and
489 Aparicio, O. M. (2012). Forkhead Transcription Factors Establish Origin Timing and Long-Range
490 Clustering in S. cerevisiae. Cell *148*, 99-111.

491 Kouprina, N., Kroll, E., Bannikov, V., Bliskovsky, V., Gizatullin, R., Kirillov, A., Shestopalov, B.,
492 Zakharyev, V., Hieter, P., and Spencer, F. (1992). CTF4 (CHL15) mutants exhibit defective DNA
493 metabolism in the yeast Saccharomyces cerevisiae. Mol Cell Biol *12*, 5736-5747.

494 Kunkel, T. A. (2011). Balancing eukaryotic replication asymmetry with replication fidelity. Curr
495 Opin Chem Biol *15*, 620-626.

496 Kunkel, T. A., and Burgers, P. M. (2008). Dividing the workload at a eukaryotic replication fork.
497 Trends Cell Biol *18*, 521-527.

498 Kurat, C. F., Yeeles, J. T., Patel, H., Early, A., and Diffley, J. F. (2017). Chromatin Controls DNA
499 Replication Origin Selection, Lagging-Strand Synthesis, and Replication Fork Rates. Mol Cell
500 *65*, 117-130.

501 Kwan, E. X., Wang, X. S., Amemiya, H. M., Brewer, B. J., and Raghuraman, M. K. (2016). rDNA
502 Copy Number Variants Are Frequent Passenger Mutations in Saccharomyces cerevisiae
503 Deletion Collections and de Novo Transformants. G3 (Bethesda) *6*, 2829-2838.

504 Lemoine, F. J., Degtyareva, N. P., Lobachev, K., and Petes, T. D. (2005). Chromosomal
505 translocations in yeast induced by low levels of DNA polymerase a model for chromosome
506 fragile sites. Cell *120*, 587-598.

507 McGuffee, S. R., Smith, D. J., and Whitehouse, I. (2013). Quantitative, Genome-Wide Analysis
508 of Eukaryotic Replication Initiation and Termination. Mol Cell *50*, 123-135.

509 Miyabe, I., Mizuno, K., Keszthelyi, A., Daigaku, Y., Skouteri, M., Mohebi, S., Kunkel, T. A.,
510 Murray, J. M., and Carr, A. M. (2015). Polymerase δ replicates both strands after homologous
511 recombination-dependent fork restart. Nat Struct Mol Biol *22*, 932-938.

512 Muzi Falconi, M., Piseri, A., Ferrari, M., Lucchini, G., Plevani, P., and Foiani, M. (1993). De novo
513 synthesis of budding yeast DNA polymerase alpha and POL1 transcription at the G1/S

514 boundary are not required for entrance into S phase. Proc Natl Acad Sci U S A *90*, 10519-
515 10523.

516 Ogawa, T., and Okazaki, T. (1980). Discontinuous DNA replication. Annu Rev Biochem *49*, 421-
517 457.

518 Osborn, A. J., and Elledge, S. J. (2003). Mrc1 is a replication fork component whose
519 phosphorylation in response to DNA replication stress activates Rad53. Genes Dev *17*, 1755-
520 1767.

521 Osmundson, J. S., Kumar, J., Yeung, R., and Smith, D. J. (2017). Pif1-family helicases
522 cooperatively suppress widespread replication-fork arrest at tRNA genes. Nat Struct Mol Biol
523 *24*, 162-170.

524 Petryk, N., Kahli, M., d'Aubenton-Carafa, Y., Jaszczyszyn, Y., Shen, Y., Silvain, M., Thermes,
525 C., Chen, C. L., and Hyrien, O. (2016). Replication landscape of the human genome. Nat
526 Commun *7*, 10208.

527 Pourkarimi, E., Bellush, J. M., and Whitehouse, I. (2016). Spatiotemporal coupling and
528 decoupling of gene transcription with DNA replication origins during embryogenesis in C.
529 elegans. Elife *5*,

530 Pursell, Z. F., Isoz, I., Lundstrom, E. B., Johansson, E., and Kunkel, T. A. (2007). Yeast DNA
531 polymerase epsilon participates in leading-strand DNA replication. Science *317*, 127-130.

532 Reijns, M. A., Kemp, H., Ding, J., de Procé, S. M., Jackson, A. P., and Taylor, M. S. (2015).
533 Lagging-strand replication shapes the mutational landscape of the genome. Nature *518*, 502-
534 506.

535 Samora, C., Saksouk, J., Goswami, P., Wade, B., Singleton, M., Bates, P., Lengronne, A.,
536 Costa, A., and Uhlmann, F. (2016). Ctf4 Links DNA Replication with Sister Chromatid Cohesion
537 Establishment by Recruiting the Chl1 Helicase to the Replisome. Molecular Cell *63*, 371-384.

538 Sasaki, M., and Kobayashi, T. (2017). Ctf4 Prevents Genome Rearrangements by Suppressing
539 DNA Double-Strand Break Formation and Its End Resection at Arrested Replication Forks.
540 Molecular Cell *66*, 533-545.e5.

541 Shah, K. A., Shishkin, A. A., Voineagu, I., Pavlov, Y. I., Shcherbakova, P. V., and Mirkin, S. M.
542 (2012). Role of DNA polymerases in repeat-mediated genome instability. Cell Rep *2*, 1088-
543 1095.

544 Shyian, M., Mattarocci, S., Albert, B., Hafner, L., Lezaja, A., Costanzo, M., Boone, C., and
545 Shore, D. (2016). Budding Yeast Rif1 Controls Genome Integrity by Inhibiting rDNA Replication.
546 PLoS Genet *12*, e1006414.

547 Simon, A. C., Zhou, J. C., Perera, R. L., van, D., Frederick, Evrin, C., Ivanova, M. E., Kilkenny,
548 M. L., Renault, L., Kjaer, S., Matak-Vinković, D., Labib, K., Costa, A., and Pellegrini, L. (2014). A
549 Ctf4 trimer couples the CMG helicase to DNA polymerase α in the eukaryotic replisome. Nature
550 *510*, 293-297.

551 Smith, D. J., and Whitehouse, I. (2012). Intrinsic coupling of lagging-strand synthesis to
552 chromatin assembly. Nature *483*, 434-438.

553 Song, W., Dominska, M., Greenwell, P. W., and Petes, T. D. (2014). Genome-wide high-
554 resolution mapping of chromosome fragile sites in Saccharomyces cerevisiae. Proc Natl Acad
555 Sci U S A *111*, E2210-8.

556 Szyjka, S. J., Viggiani, C. J., and Aparicio, O. M. (2005). Mrc1 is required for normal progression
557 of replication forks throughout chromatin in S. cerevisiae. Mol Cell *19*, 691-697.

558 Tanaka, H., Katou, Y., Yagura, M., Saitoh, K., Itoh, T., Araki, H., Bando, M., and Shirahige, K.
559 (2009). Ctf4 coordinates the progression of helicase and DNA polymerase alpha. Genes Cells
560 *14*, 807-820.

561 Taylor, M. R. G., and Yeeles, J. T. P. (2018). The Initial Response of a Eukaryotic Replisome to
562 DNA Damage. Molecular Cell *https://doi.org/10.1016/j.molcel.2018.04.022,*

563 Tran, P. L. T., Pohl, T. J., Chen, C. F., Chan, A., Pott, S., and Zakian, V. A. (2017). PIF1 family
564 DNA helicases suppress R-loop mediated genome instability at tRNA genes. Nat Commun *8*,
565 15025.

566 Villa, F., Simon, A. C., Ortiz Bazan, M. A., Kilkenny, M. L., Wirthensohn, D., Wightman, M.,
567 Matak-Vinkovíc, D., Pellegrini, L., and Labib, K. (2016). Ctf4 Is a Hub in the Eukaryotic
568 Replisome that Links Multiple CIP-Box Proteins to the CMG Helicase. Mol Cell *63*, 385-396.

569 Wu, C. A., Zechner, E. L., Reems, J. A., McHenry, C. S., and Marians, K. J. (1992). Coordinated
570 leading- and lagging-strand synthesis at the Escherichia coli DNA replication fork. V. Primase
571 action regulates the cycle of Okazaki fragment synthesis. J Biol Chem *267*, 4074-4083.

572 Yadav, T., and Whitehouse, I. (2016). Replication-Coupled Nucleosome Assembly and
573 Positioning by ATP-Dependent Chromatin-Remodeling Enzymes. Cell Rep

574 Yeeles, J. T., Janska, A., Early, A., and Diffley, J. F. (2017). How the Eukaryotic Replisome
575 Achieves Rapid and Efficient DNA Replication. Mol Cell *65*, 105-116.

576 Yoshida, K., Bacal, J., Desmarais, D., Padioleau, I., Tsaponina, O., Chabes, A., Pantesco, V.,
577 Dubois, E., Parrinello, H., Skrzypczak, M., Ginalski, K., Lengronne, A., and Pasero, P. (2014).
578 The histone deacetylases sir2 and rpd3 act on ribosomal DNA to control the replication program
579 in budding yeast. Mol Cell *54*, 691-697.

580 Zhu, W., Ukomadu, C., Jha, S., Senga, T., Dhar, S. K., Wohlschlegel, J. A., Nutt, L. K.,
581 Kornbluth, S., and Dutta, A. (2007). Mcm10 and And-1/CTF4 recruit DNA polymerase alpha to
582 chromatin for initiation of DNA replication. Genes Dev *21*, 2288-2299.

583

Porcella et al., Figure 1

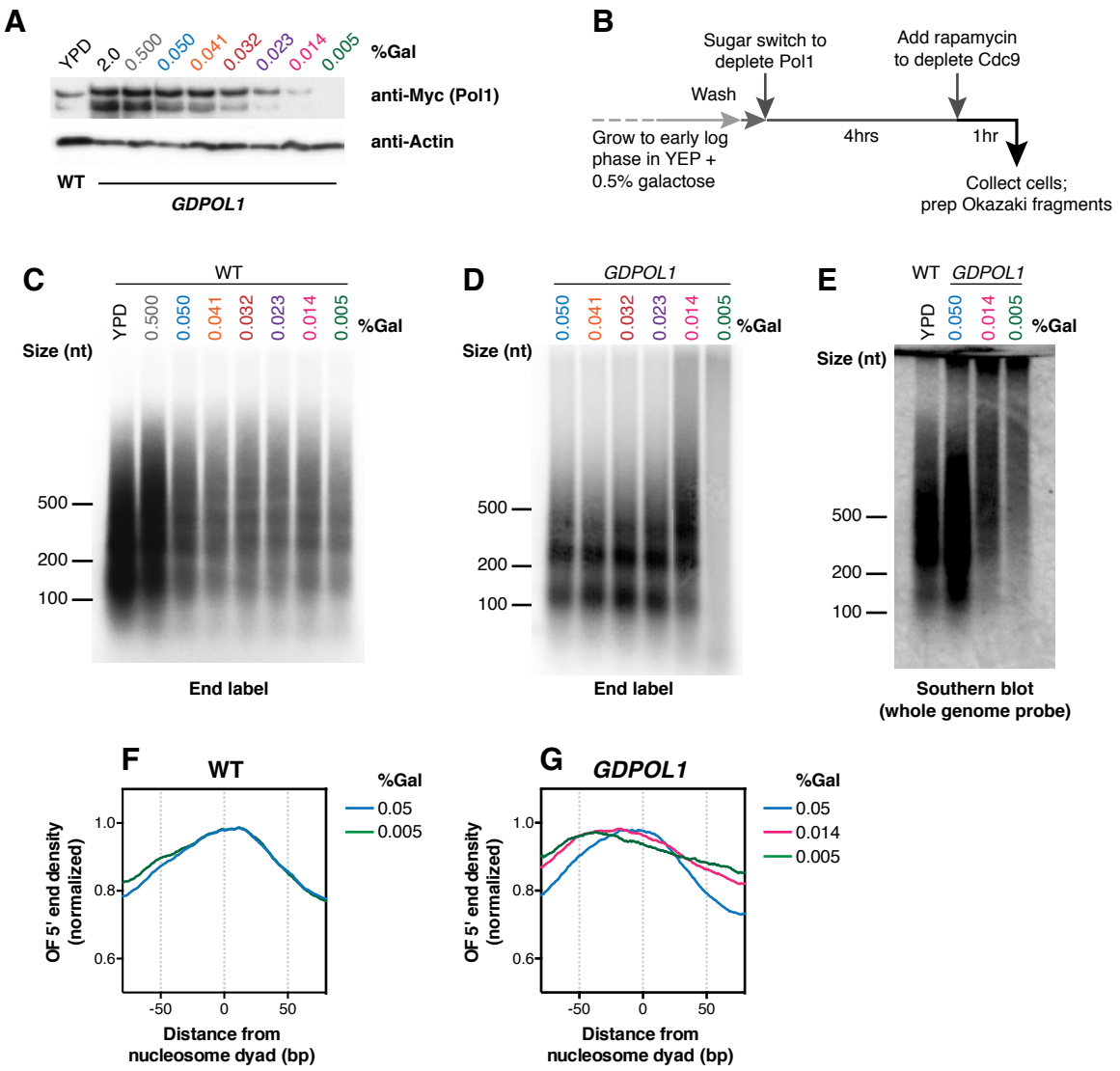

Figure 1. Okazaki fragments increase in length when Pol α is limiting.

(A). Western blot against 13xMyc-tagged Pol1 from S. cerevisiae from a wild-type or *GDPOL1* strain, as indicated, shifted to YPD or YEP + 3% raffinose (hereafter, media) supplemented with various concentrations of galactose

(B). Schematic of experimental workflow for Okazaki fragment analysis and sequencing (also see methods)

(C, D). Alkaline agarose gel analysis of end-labeled Okazaki fragments from a wild-type (C) or *GDPOL1* (D) strain, shifted to YPD or media supplemented with galactose as indicated.

(E). Southern blot using a whole genome probe, on Okazaki fragments from a wild-type or *GDPOL1* strain shifted to media with the indicated sugar concentrations.

(F, G). Distribution of Okazaki fragment termini around consensus nucleosome dyads (Jiang and Pugh, 2009) for a wild-type (F) or *GDPOL1* (G) strain shifted to media containing 0.05% (blue), 0.014% (pink), or 0.005% (green) galactose.

Porcella et al., Figure 2

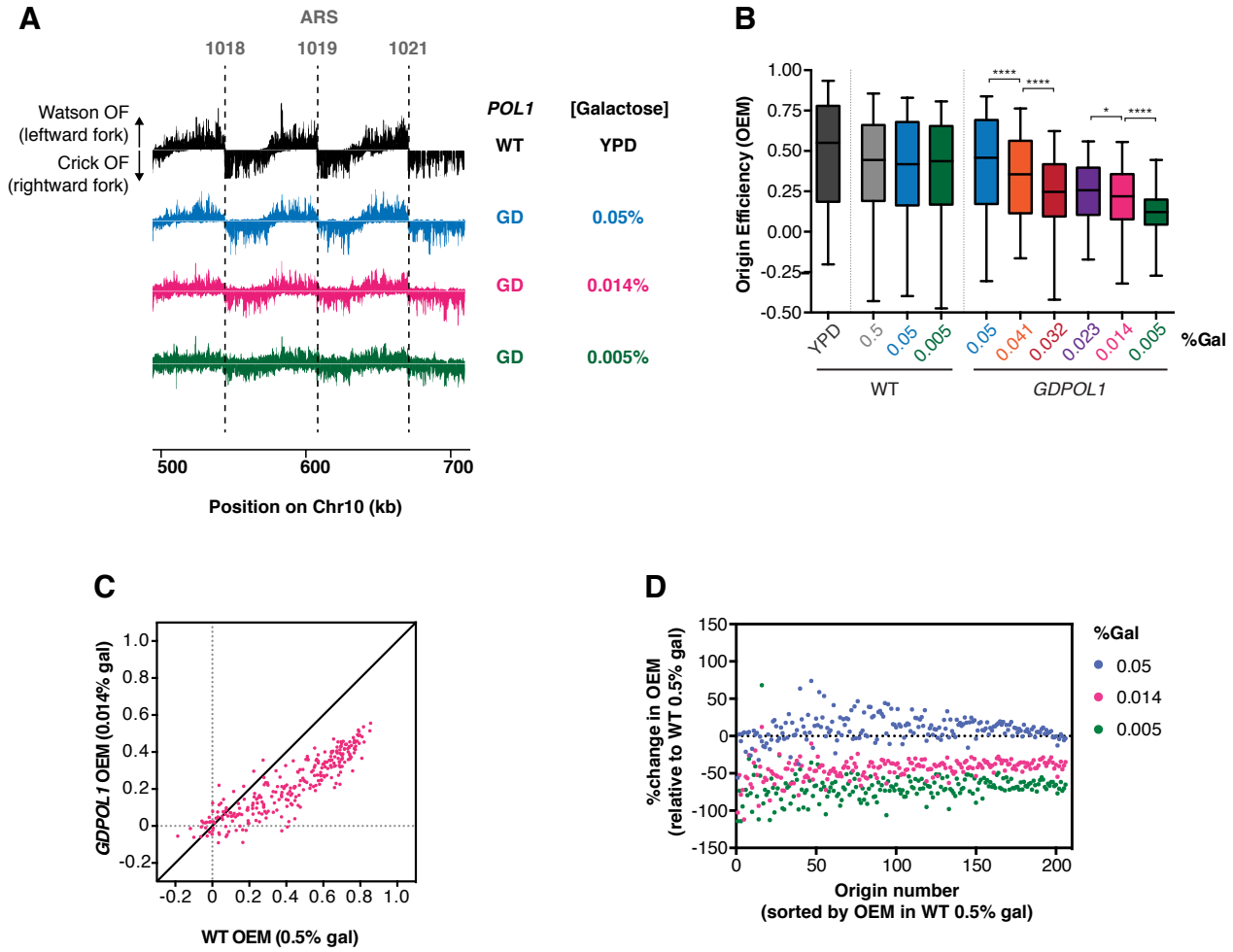

Figure 2. Origin firing efficiency is decreased for all replication origins when Pol α levels are reduced

(A). Okazaki fragment distributions from a wild-type (black) or *GDPOL1* strain shifted to the indicated media. A ~200 kb region from the right arm of chromosome 10 is shown, and three efficient origins are annotated.

(B). Origin efficiency in wild-type or GDPOL1 cells shifted to the indicated concentration of galactose. Origin efficiency was calculated as in (McGuffee et al., 2013), using origin locations annotated in the same study. Significance was calculated by unpaired t-test; **** $p<0.0001$, * $p<0.05$. Data from the *GDPOL1* strain are the average of two replicates.

(C). Scatter plot comparing origin firing efficiency in *GDPOL*1 cells at 0.014% galactose, to wild-type cells in 0.5% galactose. Analogous comparisons to other galactose concentrations, and correlations between replicates, are in Fig. S2.

(D). Scatter plot showing the percentage decrease in origin firing efficiency, relative to wild-type cells, for *GDPOL1* cells shifted to the indicated galactose concentrations. Origins were ordered by their firing efficiency in wild-type cells at 0.5% galactose. Each origin efficiency spot represents the average of two replicates.

Porcella et al., Figure 3

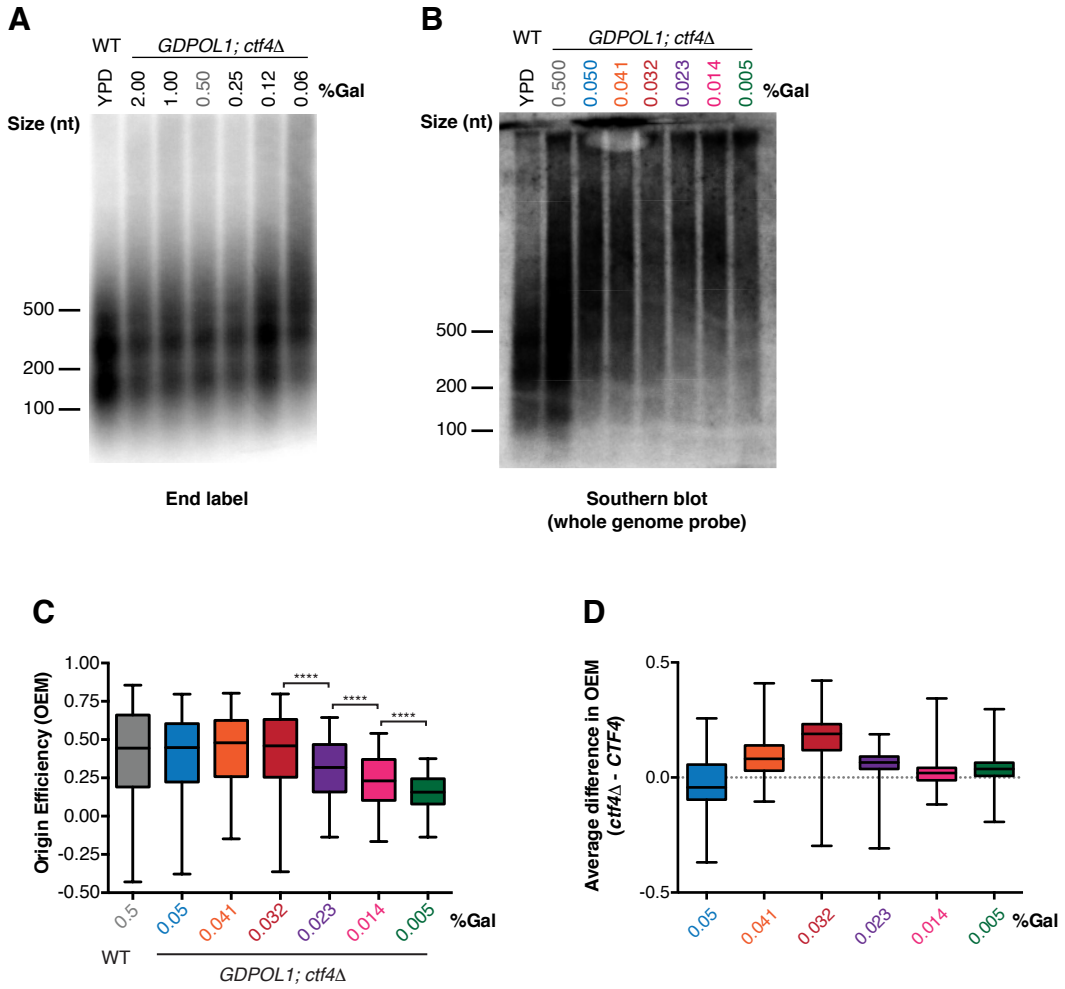

Figure 3. Ctf4 maintains Okazaki fragment length at low Pol α concentrations but is dispensable for origin firing in vivo

(A). Alkaline agarose gel analysis of end-labeled Okazaki fragments from a wild-type or *GDPOL1;ctf4*Δ strain, as indicated, shifted to media containing various concentrations of galactose. Note that the range of galactose concentrations here is significantly higher than in other figure panels.

(B). Southern blot using a whole genome probe, on Okazaki fragments from a wild-type or *GDPOL1;ctf4*Δ strain shifted to media shifted to low galactose concentrations.

(C). Replication origin efficiency, as in Fig. 2B, for *GDPOL1;ctf4*Δ cells at low galactose concentrations. Data were calculated and analyzed as in Fig. 2B

(D). Comparison of origin efficiencies for *CTF4* vs *ctf4*Δ strains shifted to identical media

Porcella et al., Figure 4

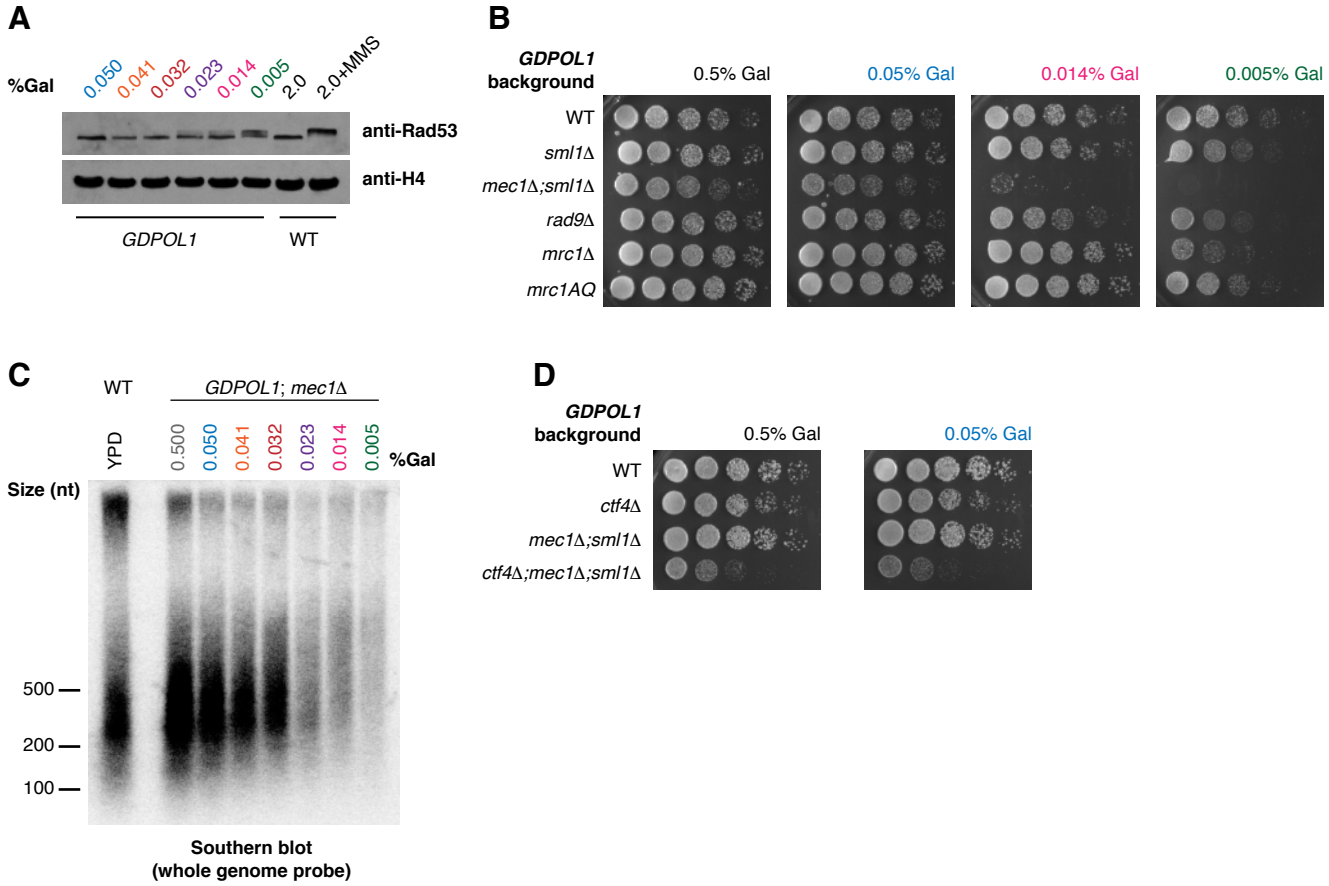

Figure 4. The checkpoint is required for viability under conditions of limiting origin firing, but not increased Okazaki fragment size.

(A). Western blot against Rad53 from *GDPOL1* cells shifted to the indicated media. A wild-type strain grown in YPD ± 0.1% MMS were used as negative and positive controls for Rad53 hyperphosphorylation

(B). Serial dilution spot tests to assay the growth of *GDPOL1* strains carrying additional mutations (*mec1*Δ;*sml1*Δ, *rad9*Δ, *mrc1*Δ and *mrc1AQ*) at the indicated galactose concentrations.

(C). Southern blot as in Fig. 3B, for a *mec1*Δ;*GDPOL1* strain shifted to various galactose concentrations.

(D). Serial dilution spot tests to assay the growth of *ctf4*Δ;*GDPOL1* strains with or without additional deletion of *MEC1*.

Porcella et al., Figure 5

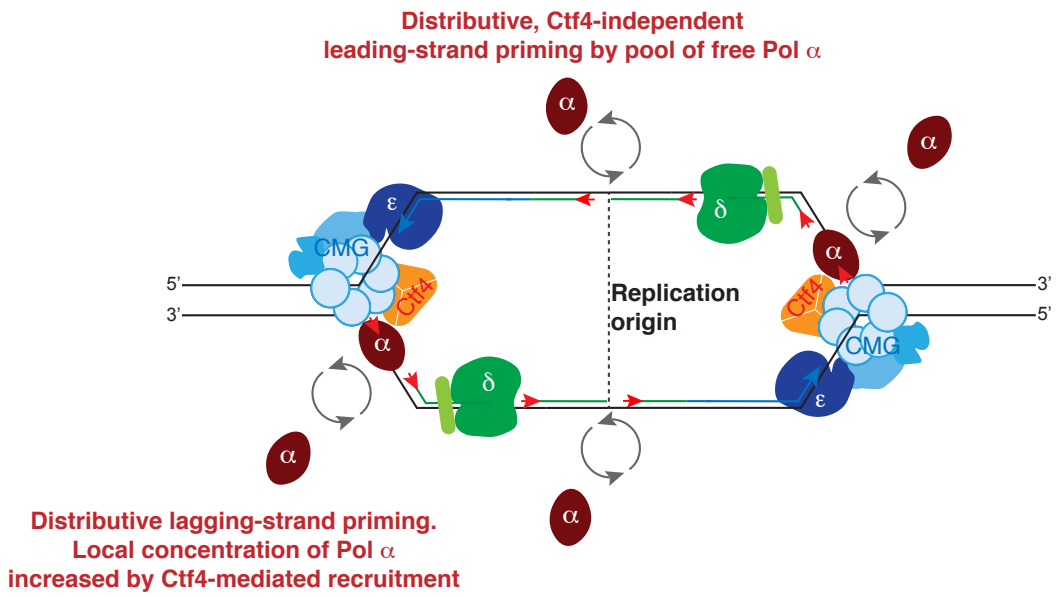

Figure 5. Model of Pol α recruitment for leading- and lagging-strand priming in *S. cerevisiae*

Porcella et al., Figure S1, associated with Figure 1

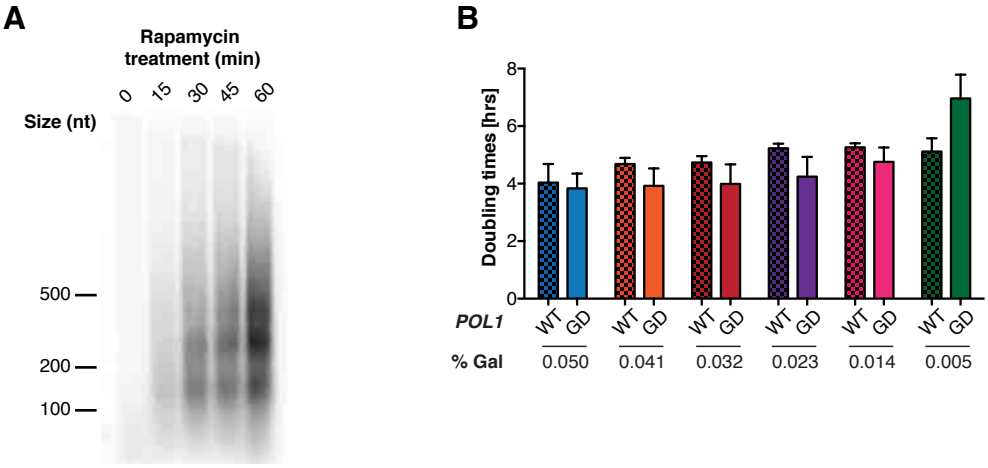

Figure S1 (Associated with Fig 1)

(A). Timecourse of Okazaki fragment enrichment during Cdc9 nuclear depletion by anchor away (Haruki et al., 2008). Okazaki fragments were prepared and labeled as in Fig. 1C, and as previously described (Smith and Whitehouse, 2012).

(B). Doubling times for wild-type or *GDPOL1* strains in YEP + 3% raffinose, supplemented with the indicated concentration of galactose. Data are the average of at least three replicates in each case.

Porcella et al., Figure S2, associated with Figure 2

A **OEM correlations across replicates**

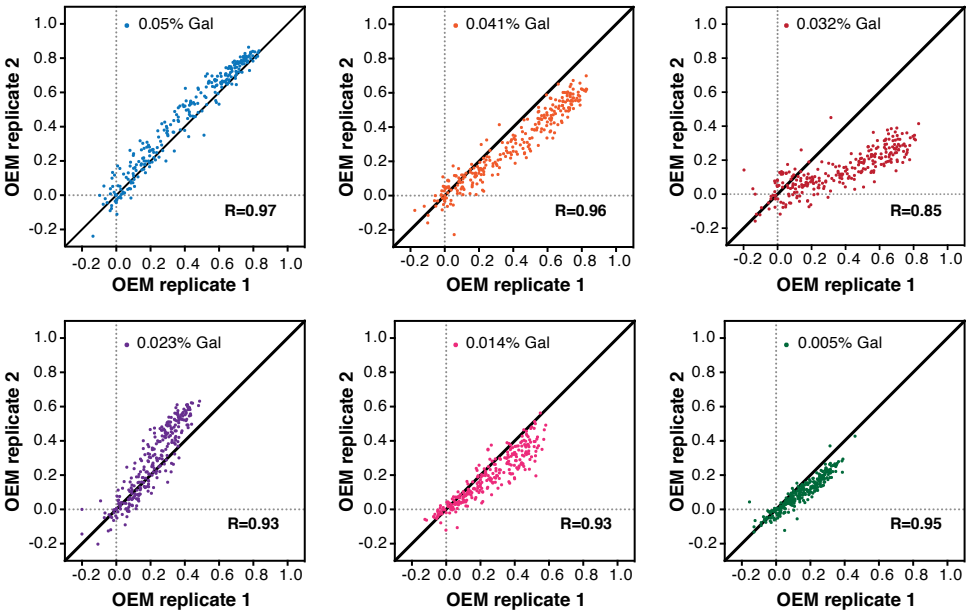

B **OEM change relative to unperturbed cells**

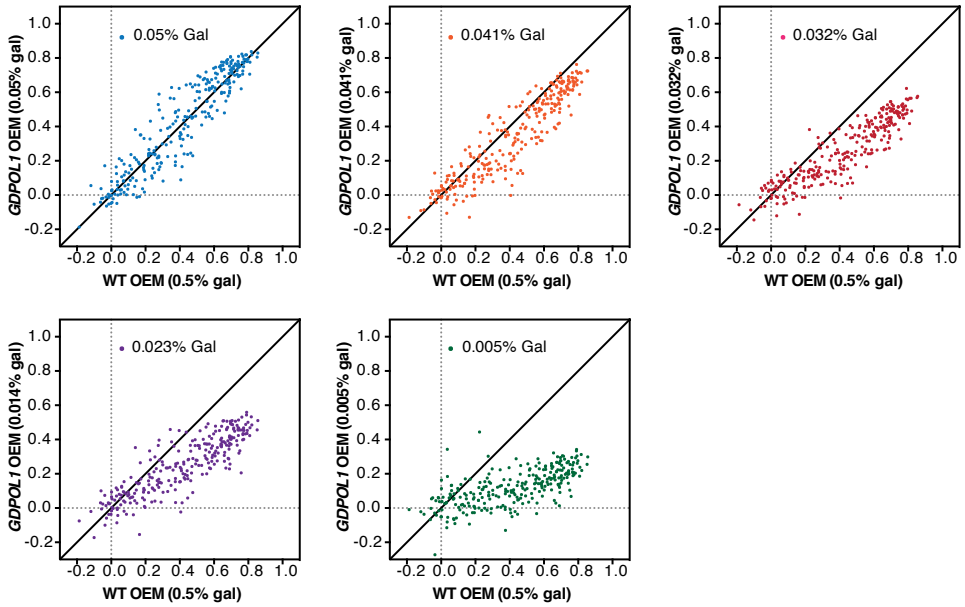

Figure S2 (Associated with Fig 2)

(A). Origin efficiency replicate comparisons for data from the *GDPOL1* strain shown in Fig. 2B.

(B). Scatter plots comparing origin firing efficiency in *GDPOL1* cells at various galactose concentrations, to wild-type cells in 0.5% galactose. Data from 0.014% are shown in Figure 2C.

Porcella et al., Figure S3, associated with Figure 2

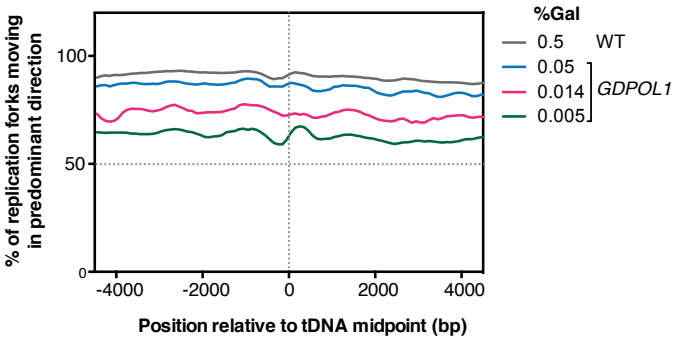

Figure S3 (Associated with Fig 2)

Analysis of replication-fork direction around 93 origin-distal tRNA genes (Osmundson et al., 2017) in *GDPOL*1 cells grown at various galactose concentrations. Increased replication-fork stalling or arrest at these sites would manifest as a decrease at or after the midpoint of the gene (Osmundson et al., 2017).

Porcella et al., Figure S4, associated with Figure 3

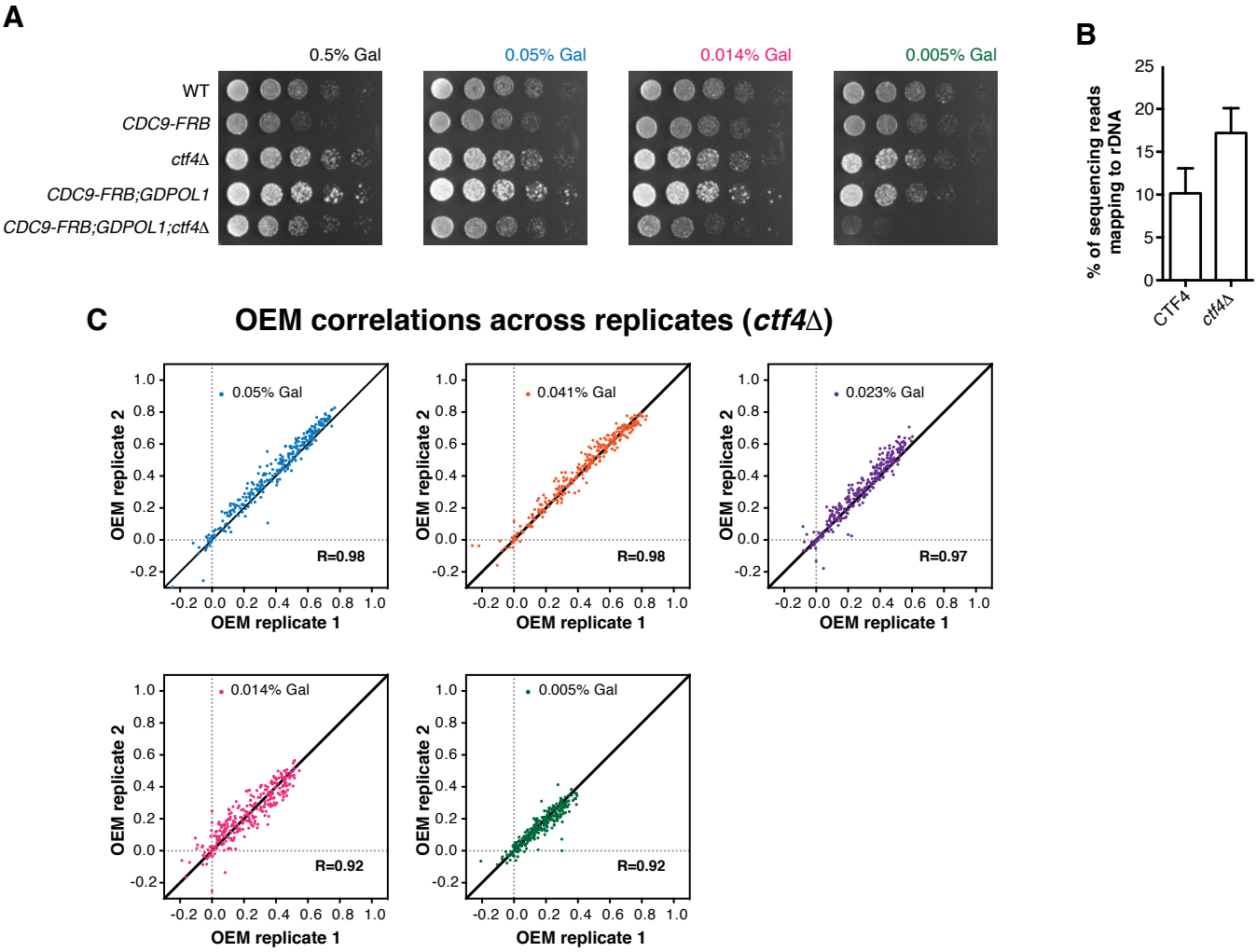

Figure S4 (Associated with Fig 3)

(A). Serial dilution spot tests to assay the growth of *GDPOL1* strains with or without FRB tagging of *CDC9* and/or additional deletion of *CTF4*.

(B). The rDNA repeat is expanded in *ctf4*Δ;*GDPOL1* cells. The proportion of sequencing reads mapping to the rDNA is indicated. Data represent the mean ± SD of all sequencing datasets used for analysis in figures 2&3.

(C). Origin efficiency replicate comparisons for data from the *ctf4*Δ;*GDPOL1* strain shown in Fig. 3C.